# Three-Dimensional Polymeric Scaffold Based Current Collector for Lithium Metal Anode toward High Energy Density Batteries

| | |
|---|---|
| Journal: | *ACS Energy Letters* |
| Manuscript ID | nz-2023-027527.R1 |
| Manuscript Type: | Letter |
| Date Submitted by the Author: | 22-Jan-2024 |
| Complete List of Authors: | Kim, Ju-Myung; Pacific Northwest National Laboratory,<br>Jia, Hao; PNNL, Energy and Environment Directorate<br>Koirala, Krishna Prasad; Pacific Northwest National Laboratory, Physical and Computational Sciences Directorate<br>Liu, DIanying; Pacific Northwest National Laboratory<br>Simmons, Ashley; Argonne National Laboratory<br>Engelhard, Mark; Pacific Northwest National Laboratory, EMSL<br>Ahmed, Ridwan; Pacific Northwest National Laboratory, Energy and Environment Directorate<br>Zhang, Yuepeng; Argonne National Laboratory, Applied Materials Division<br>Wang, Chongmin; Pacific Northwest National Laboratory, EMSL<br>Zhang, Ji-Guang; Pacific Northwest National Laboratory, Energy and Environment Directorate<br>Xu, Wu; Pacific Northwest National Laboratory, Energy and Environment Directorate |
| | |

# Three-Dimensional Polymeric Scaffold Based Current Collector for Lithium Metal Anode toward High Energy Density Batteries

*Ju-Myung Kim[1#], Hao Jia[1#], Krishna Prasad Koirala[2], Dianying Liu[1], Ashley Simmons[3], Mark H. Engelhard[1], Ridwan A. Ahmed[1], Yuepeng Zhang[3], Chongmin Wang[4], Ji-Guang Zhang[1*], Wu Xu[1*]*

[1] Energy and Environment Directorate, Pacific Northwest National Laboratory, Richland, WA 99354, USA

[2] Physical and Computational Sciences Directorate, Pacific Northwest National Laboratory, Richland, WA 99354, USA

[3] Applied Materials Division, Argonne National Laboratory, Lemont, IL 60439, USA

[4] Environmental and Molecular Sciences Laboratory, Pacific Northwest National Laboratory, Richland, WA 99354, USA

[#] These authors contributed equally.

[*] Corresponding authors. Email: jiguang.zhang@pnnl.gov; wu.xu@pnnl.gov

## ABSTRACT

The practical applications of high energy density rechargeable lithium (Li) metal batteries (LMBs) have been impeded by the intrinsic issues of Li metal anode (LMA) including high reactivity with electrolyte and dendritic formation. Conventional LMAs which have the "hostless" feature consisting of a Li layer on the two-dimensional copper (Cu) foil as a current collector led to additional loss in specific energy density since Cu is a non-faradaic heavy metal, bringing the formidable areal capacity loss. To address these problems, the heat-treated 3D-structured Cu-coated polyimide (HT-Cu@PI) membrane is designed and fabricated as a current collector. Benefiting from this unique material/structure, it enables not only better electrochemically deposited Li by uniform/continuous Li-ion transport pathway but significant increase in the gravimetric/volumetric energy densities of LMBs by allowing more Li deposition in a fixed weight/volume. Therefore, this new LMA structure will accelerate the practical application of the high energy density LMBs.


Table of Content Graphic

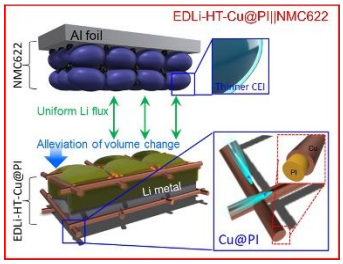

Demands for high energy density rechargeable batteries have been continuously increasing with the rapid market penetration of electric vehicles and portable electronic devices. Although lithium (Li)-ion batteries (LIBs) have been widely used as the primary energy sources in these applications, their gravimetric and volumetric energy densities eventually reach the limit of graphite anode. [1-3] In this regard, Li metal has been considered one of the most promising anode materials due to its high theoretical specific capacity (3860 mAh $g^{-1}$) which is ten times of graphite anode (~ 372 mAh $g^{-1}$) currently used in the state-of-the-art LIBs and its lowest electrochemical reduction potential (−3.040 V vs standard hydrogen electrode). [4, 5] However, the practical applications of Li metal anodes (LMAs) are significantly hampered because of several intrinsic issues including high reactivity of Li and formation of dendritic Li, which cause low Li Coulombic efficiency (CE), continuous loss of Li and electrolyte, accumulation of nonuniform/unstable solid electrolyte interphase (SEI) layer, formation of electrochemical inactive or "dead" Li during repeated Li deposition and stripping, and consequently short cycle life and safety concern. [6-8]

From the structural point of view, the conventional LMA consists of a Li metal foil on the top of a two-dimensional (2D) copper (Cu) foil. The presence of the Cu current collector accommodates a portion of the LMA mass, and it leads to the formidable loss of the areal capacity and specific energy density since Cu is non-faradaic and one of the heavy metals. In addition, the "hostless" feature of LMA gives rise to further issues including volume expansion and the limited utilization of Li. [9, 10] To solve the abovementioned obstacles, several efforts have been devoted to developing a three-dimensional (3D) substrate as the alternative current collector of the 2D Cu foil. One of the previous approaches can be categorized as the carbon-based hosts (ex. carbon nanotubes[11, 12], carbon fibers[13, 14], and graphene[15, 16]) that could have electrolyte wettability issues. Another is the nanostructured 3D metallic substrates (ex. metal mesh [17, 18], metal foam [19, 20], and the modified 3D metal substrate with lithocholic materials[21-24]). Even though the 3D metallic substrates brought improvements in the electrochemical performance, there are still concerns about the restricted mass of the loaded Li metal inside due to their intrinsic heavyweight. As a strategy to reduce the weight of the metal current collectors used in LIBs, lightweight polymeric membranes such as poly(ethylene naphthalate), poly(ethylene terephthalate), poly(ether sulfone), and polyimide (PI) have been used as the substrates to coat with metal films on them and Cu has been mostly preferred as the electronic conduction-pathway provider. [25, 26] Although the double-side Cu-coated PI membranes were reported as lightweight current collectors because of PI's good

mechanical properties and high thermal stability [27, 28], usage of such Cu-coated polymer current collectors is limited to LIBs based on the best of our knowledge and they stick with a 2D substrate. Recently, Wu et al.,[29] reported a 3D substrate by electroless plating Cu on a PI film with through hole arrays drilled using laser and used it for the $Li_4Ti_5O_{12}$ anode to increase the portion of the active material in the entire electrode and consequently the energy density of LIBs.

Here, we propose a 3D Cu-coated polymeric scaffold prepared by electrospinning as the current collector to address the long-standing challenges of LMAs. Electrospinning is known as one of the facile and versatile processes to fabricate a polymeric nanomat and it can adopt a variety of polymers according to needs. Electrospun PI was selected as the polymeric scaffold based on its high thermal stability (>500 ºC) and Cu was chosen as the provider of the electronic conduction pathway. The 3D Cu-coated PI (Cu@PI) current collector is produced via electroless plating in an aqueous solution containing Cu ions. Well-distributed Cu nanoparticles on PI nanofibers are confirmed by scanning electron microscope (SEM) and energy-dispersive X-ray spectroscopy (EDS). To further enhance the electronic conductivity of Cu@PI, the heat-treated 3D Cu@PI current collector enables dense deposition of Li during cycling and enhances the electrochemical performance of LMBs by uniform and continuous Li-ion transport pathway through the porous substrate. It also improved the gravimetric/volumetric energy densities of LMBs due to the reduced weight and the stable framework of the composite current collector. This new strategy of 3D LMAs would facilitate the commercial application of the high energy density LMBs.

**Optimization of the Cu@PI 3D Current Collector**

The Cu@PI nanomat was prepared by an electroless plating method as shown in Figure S1. Ring-opening of imide in PI happens when it meets with a base solution such as KOH and PI-$COO^-$-$K^+$ is formed. $K^+$ can be changed to $Ag^+$ after simple immersing in an $AgNO_3$ solution and PI-$COO^-$-$Ag^+$ is chemically reduced to Ag nanoparticles by a reducing agent. Then Ag-coated PI is soaked into an electroless plating solution of Cu ions to coat Cu nanoparticles on the PI. The detail is further described in the Experimental method. The electrospun PI nanomat with 30 μm thickness was used as the 3D substrate for this study. To check if the Cu nanoparticles are well-coated on PI nanofibers, SEM imaging and EDS mapping were conducted. It is found that submicron-size Cu nanoparticles are uniformly distributed on the PI nanofibers by SEM (Figure 1a) and the Cu

element is detected along with the PI nanofibers by EDS (Figure S1b). The 12-μm thick commercial 2D Cu foil was used as a control. As shown in Table S1, the 2D Cu foil has an electronic conductivity of $5.88 \times 10^5$ S cm$^{-1}$ while the fabricated Cu@PI in this work has an electronic conductivity of $1.97 \times 10^3$ S cm$^{-1}$. When the 5 mAh cm$^{-2}$ of Li was deposited on Cu@PI at a current density of 0.5 mA cm$^{-2}$ (=C/10) in an electrolyte of Li bis(fluorosulfonyl)imide (LiFSI) in 1,2-dimethoxyethane (DME) and 1,1,2,2-tetrafluoroethyl-2,2,3,3-tetrafluoropropyl ether (TTE) (at 1:1.2:3 by mol.), the deposited Li stayed on the top of the substrate and didn't go through the thickness direction (Figure 1b). Also, the overpotential of Cu@PI during Li deposition is close to that of the bare Li as shown in Figure 1c.

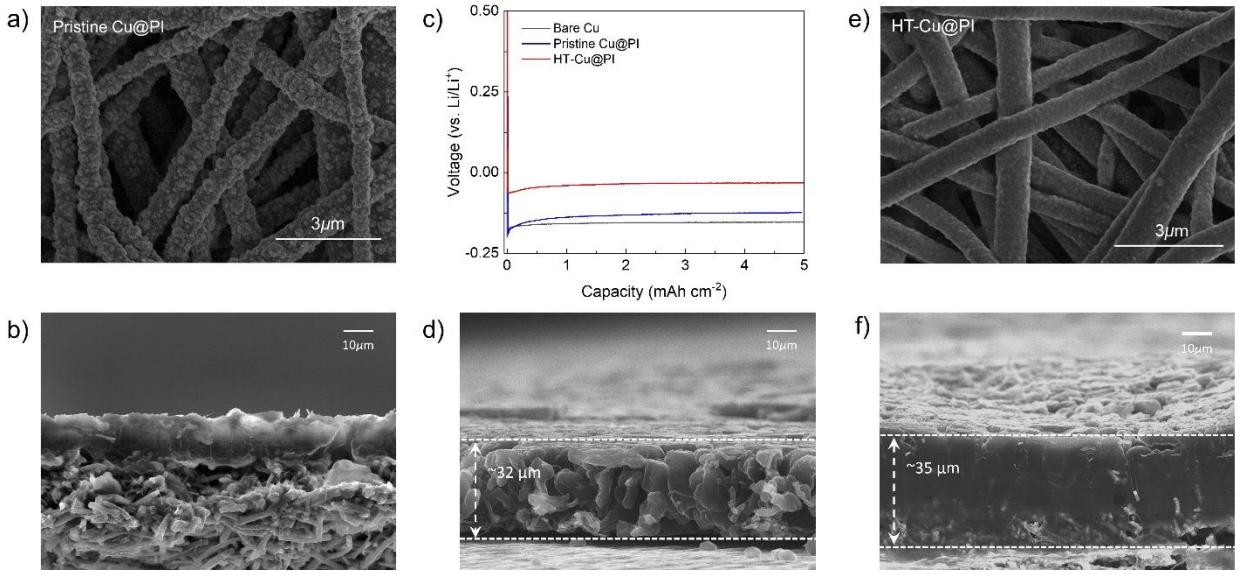


**Figure 1.** SEM images of a) surface-view of Pristine Cu@PI and b) cross-sectional view of EDLi-Pristine Cu@PI. c) Li deposition profiles in Li||Cu cells for a capacity of 5 mAh cm$^{-2}$ at a current density of 0.5 mA cm$^{-2}$. d) A cross-sectional SEM image of EDLi-Bare Cu. SEM images of e) surface-view of HT-Cu@PI and f) cross-sectional view of EDLi-HT-Cu@PI.

The thermal annealing at around 200 °C of electroless-plated Cu on the substrate is known for improving its electronic conductivity which could help Li deposition. [30, 31] Therefore, the as-prepared Cu@PI nanomat were annealed at various temperatures of 150, 200, and 250 °C for 1 hour (h) under argon (Ar) flow. Cu nanoparticles tend to grow and appear smoother after the heat treatment compared to the pristine Cu@PI (Figure S2a – S2d) due to reductions in grain boundary resulting in a slight enhancement of electronic conductivity (Table S1).[31] Therefore, 200 °C was

chosen as the optimal annealing temperature because it led to the highest electronic conductivity (~2.69 × $10^3$ S $cm^{-1}$) and could avoid the possible decomposition of PI. To further optimize the annealing condition, the heat-treating time was extended to 5 and 10 h. Although the electronic conductivity of the heat-treated Cu@PI at 200 °C decreased a bit with annealing time from 1 to 10 h (Table S1), the Cu@PI annealed at 200 °C for 10 h exhibited the smoothest surface by the interconnection of the Cu nanoparticles (Figure S2c, S2e, and S2f). It is expected that a smoother surface will help improve the Li deposition uniformly on the substrate. [32] The cross-sectional SEM image of HT-Cu@PI confirms that Cu nanoparticles are coated through the thickness direction as well (Figure S3).

To elucidate the effect of the heat treatment on Cu@PI, Li (5 mAh $cm^{-2}$) was deposited on the annealed Cu@PI nanomat at the current density of 0.5 mA $cm^{-2}$ (=C/10), the same deposition condition as for the pristine Cu@PI and bare Cu foil. The cross-sectional SEM images of Cu@PI annealed under various temperatures and times exhibit clear differences (Figure S4). In this work, Cu elements detected by EDS mapping on the backside of the Cu@PI nanomat is used as an effective criteria for the uniformity of Li deposition through the thickness direction of the nanomat: If no Cu can be detected by EDS mapping from the backside of lithiated nanomat, it means Li can penetrate the full depth of nanomat and fully cover it. In contrast, if significant amount of Cu can be detected, it means Li did not cover the full depth of nanomat. In the case of 1 h treatment, Cu@PI annealed at 200 °C (Figure S4c) allows more Li to pass through the thickness direction and deposit inside of Cu@PI compared to other temperatures (150 and 250 °C, Figure S4b and S4d). For the Cu@PI treatment at a given temperature (such as 200°C), extending heating time from 1 to 10 h promotes Li deposition to the inside of Cu@PI (Figure S4c, S4e, and S4f). Further increasing heat treatment temperature of Cu@PI (at 250 °C) may shrink the structure of nanomat or even sinter Cu particles as shown in Figure S5. This will block Li diffusion path and lead to less Li coverage, i.e., more Cu exposure as shown in Figure S4d. In the case of 10 h treatment at 200 °C, Cu elements are barely detected by EDS mapping on the backside of the Cu@PI (Figure S4f) indicating the deposited Li fully covered bottom side of nanomat, while in other cases various amount of Cu element have been detected (Figure S4a-S4e). Based on these results, the Cu@PI treated at 200 °C for 10 h has been identified as the optimized 3D current collector (referred to HT-Cu@PI) in this study.

Compared to the pristine Cu@PI and bare Cu, the HT-Cu@PI leads to a lower polarization during Li deposition as shown in Fig. 1c. This indicates that the well-developed 3D substrate with a smoother surface brings more abundant nucleation sites that lower Li deposition potential. The thickness of 5 mAh $cm^{-2}$ Li deposited on bare Cu is ~ 32 μm by SEM (Figure 1d). The difference between the theoretical thickness of Li deposition (~ 25 μm) and the practical value observed can be attributed to the side reactions between Li and electrolyte and SEI formation. Although the thickness of Li deposited on HT-Cu@PI (~ 35 μm, see Fig. 1f) is larger than that on bare Cu with the same amount of Li deposition, it is probably because the thickness of fresh HT-Cu@PI is already ~30 μm (Figure S3a). Li deposition and stripping accommodate inevitable Li loss by SEI formation and side reactions between the electrolyte and Li. [33, 34] A small difference in the thickness of the deposited Li indicates that the side reactions between Li and electrolyte is small. This is consistent with the high efficiency electrolyte used in this work (LiFSI-1.2DME-3TTE (by mol) has a high average Li CE of 99.5%).[35] After 80% of Li stripping, the thickness of deposited Li on bare Cu decreased from ~ 32 μm to ~ 22 μm (about 31.3% shrinkage) and voids are observed in both surface and cross-sectional view images (Figure S6a). SEI layers are found as well around the voids that have the same size as the deposited Li (~ 10 μm). On the other hand, HT-Cu@PI leads to only 8.6% change in thickness (from 35 to 32 μm) after 80% of Li stripping (Figure S6b) after stripping, demonstrating a well-maintained structure for the HT-Cu@PI as a substrate, which is good for the stability of LMAs during cycling. Similar to bare Cu, the cross-sectional image of HT-Cu@PI after stripping displays the voids of Li, and Cu@PI nanofibers are exposed due to the stripping of Li even though some parts are covered by SEI layers (Figure S6b). It is confirmed that the metallic Li particles grow inside HT-Cu@PI and are stripped well due to its high electronic conductivity.

**Electrochemical Performance of Li Metal Batteries**

To investigate the effect of the optimally annealed Cu@PI (i.e. HT-Cu@PI) on the electrochemical performance of LMBs, the electrochemically deposited Li (EDLi) of 5 mAh $cm^{-2}$ on the two Cu substrates (bare Cu and HT-Cu@PI) was separately paired with $LiNi_{0.6}Mn_{0.2}Co_{0.2}O_2$ (NMC622) (4.5 mAh $cm^{-2}$) to assemble coin cells, along with 20 μm thick polyethylene separator and 75 μL electrolyte. Figure 2a compares the discharge rate capability of the EDLi||NMC622 cells between

bare Cu and HT-Cu@PI. The cells were charged at C/10 (1C = 4.5 mA $cm^{-2}$) and discharged at various rates from C/10 to 1C after two cycles of formation at C/10 within the voltage range of 2.8 to 4.4 V (vs. $Li/Li^+$). The EDLi||NMC622 cells with HT-Cu@PI delivered a higher capacity of 193 mAh $cm^{-2}$ at a current density of C/10 for discharging than those with bare Cu (188 mAh $cm^{-2}$). The cell with HT-Cu@PI substrate demonstrates increased discharge capacities even at 1C discharge rate (170 mAh $cm^{-2}$ compared to those with bare Cu (160 mAh $cm^{-2}$)). It is assumed that the 3D-structured HT-Cu@PI substrate enhances Li transport by the well-connected electronic conductive nanofibers inside. A galvanostatic intermittent titration technique (GITT) analysis is conducted at C/10 charge and 1C discharge to further understand the improved Li transport. GITT results shown in Figure 2b confirm that the cells with HT-Cu@PI exhibit lower overpotentials than the cells with bare Cu upon repeated current stimuli with a relaxation time of 2 h between pulses. The charging C-rate capability test of EDLi-Cu||NMC622 was further conducted with a constant discharging rate of 0.1C and various charging rates from 0.1C to 1C. As shown in Figure S7, EDLi-HT-Cu@PI||NMC622 delivers a higher capacity (145.5 mAh $g^{-1}$) with a lower overpotential at 1C charging compared to EDLi-bare Cu||NMC622 (131.7 mAh $g^{-1}$).

The long-term cyclability of the EDLi||NMC622 cells with HT-Cu@PI and bare Cu is evaluated to further prove the practical application (Figure 2c). The initial capacities of the cells with bare Cu and HT-Cu@PI at C/10 for charging and at C/3 for discharging are 182.0 mAh $g^{-1}$ and 186.7 mAh $g^{-1}$, respectively. This result indicates that the reduced internal resistance of HT-Cu@PI cells leads to higher capacity by more Li utilization in the 3D HT-Cu@PI substrate than in the 2D Cu foil. When the capacity retention of the EDLi||NMC622 cells reached 80%, the cycle lives of the cells with bare Cu and HT-Cu@PI substrates are 126 and 180 cycles, respectively. Table S2 compares the electrochemical performance of LMBs with different substrate. It shows that cells with EDLi-Cu-based 3D substrate with the highest cathode areal capacity and smallest N/P ratio can still demonstrates good cycling stability. Especially, most of the previous studies were conducted with $LiFePO_4$ cathode, and usage of the nickel (Ni)-rich oxide cathodes (i.e., $LiNi_xMn_yCo_{1-x-y}O_2$, $x \geq 6$) which are considered as a higher capacity cathode candidate is limited. [36, 37] Even though some of them tested with Ni-rich oxide cathodes such as NMC622[38] and NMC811[21], they show either very low average capacity or short cycle life, demonstrating that the cycling performance of EDLi||NMC622 cells with HT-Cu@PI goes beyond the previously reported EDLi-Cu-based 3D substrates for LMBs even at more practical conditions.

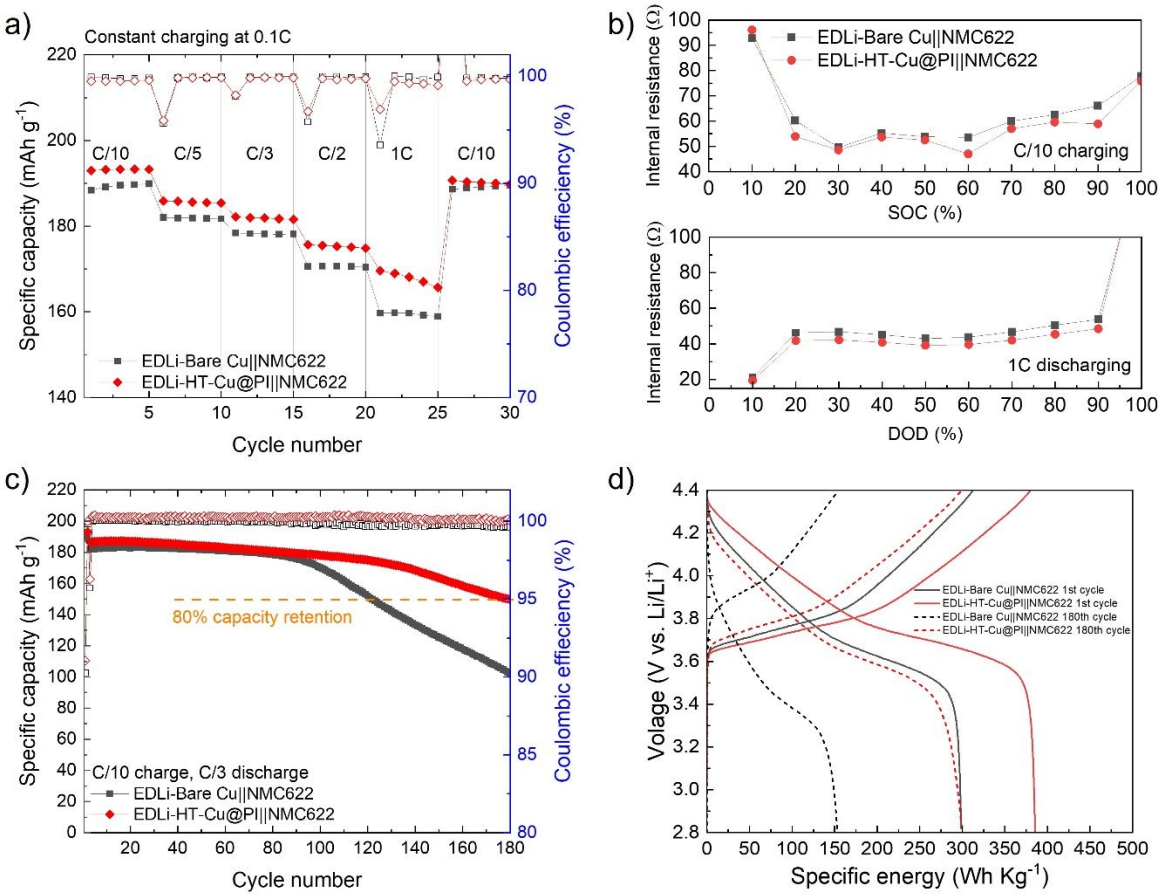


**Figure 2.** a) Discharging C-rate capability of EDLi-Cu||NMC622 (4.5 mAh $cm^{-2}$, N/P ratio = 1.11) at a constant charging rate of C/10 and at various discharging rates from C/10 to 1C under voltage range from 2.8 to 4.4 V (vs. Li/Li). b) GITT profiles of EDLi-Cu||NMC622 obtained upon the repeated current stimuli (at a C/10 charging and a 1C discharging), where the interruption time between the pulses = 5 h. c) Cycle performance of EDLi-Cu||NMC622 at a C/10 charging and a C/3 discharging. d) Charge/discharge specific energy density based on the mass of the cathode/Al substrate, separator, and EDLi/substrate (Cu or HT-Cu@PI)) on the 1st and 180th cycles.

Another significant advantage of HT-Cu@PI is the lighter substrate weight that could allow more Li metal to be stored for a fixed weight of electrodes. The mass of HT-Cu@PI is only 14.5% of the bare Cu. When 5 mAh $cm^{-2}$ of Li is deposited on various Cu substrates, EDLi-Bare Cu weights 13.98 mg $cm^{-2}$ (Li: 6.12 mg $cm^{-2}$ and Bare Cu: 7.86 mg $cm^{-2}$) with 43.7 wt.% portion of Li as shown in Figure S8. On the other hand, the weight of EDLi-HT-Cu@PI with the same amount of Li is 7.26 mg $cm^{-2}$ (Li: 6.12 mg $cm^{-2}$ and Cu@PI: 1.14 mg $cm^{-2}$) with an 84.3 wt.% portion of Li. When the total mass of the dry cell stake (including cathode/Al substrate, separator, EDLi/substrate (Cu or HT-Cu@PI)) is used to calculate the specific energy of the EDLi||NMC622

cells, the cell with HT-Cu@PI shows higher specific energy (382.4 Wh $kg^{-1}$) than that with bare Cu (299.0 Wh $kg^{-1}$) at the first cycle of Figure 2c (Figure 2d). Benefitting from the structural advantage of HT-Cu@PI, even after 180 cycles, the cells with HT-Cu@PI still deliver a specific energy of 300.5 Wh $kg^{-1}$, nearly twice for that of the cells with bare Cu (152.8 Wh $kg^{-1}$) (Figure S9a). These results indicate that the LMB using a lighter 3D current collector made of Cu-coated polymeric nanomat could improve both the cyclability and energy density of the batteries as compared to similar batteries using 2D Cu foil as the anode current collector.

**Post-Mortem Analysis of Li Metal Batteries**

The superior cycling performance of EDLi||NMC622 cells using HT-Cu@PI current collector is further verified by conducting the post-mortem analyses of the anode after 180 cycles. The electrode samples were collected from the discharged cells and thoroughly washed with fresh anhydrous DME to remove the remaining salts and solvents. The EDLi-Bare Cu (Figure 3a) presents a porous surface with a smaller size of Li particles compared to the first Li deposition (Figure S6a) indicating the dendritic Li growth during cycling. [39, 40] When compared to EDLi-Bare Cu, EDLi-HT-Cu@PI displays a smoother surface (Figure 3b). As shown in the cross-sectional SEM image of Fig. 1c, the thickness of EDLi-Bare Cu is ~ 65 μm after cycling which corresponding to a 103% volume expansion comparing to the thickness after first Li deposition (~ 32 μm, see Figure 1d). In contrast, EDLi-HT-Cu@PI alleviates the volume expansion to 68% after cycling (~ 35 μm at the first deposition to ~ 59 μm after 180 cycles, see Figure 1f and Figure 3d). When the total volume of the dry cell stake (including cathode/Al substrate, separator, EDLi/substrate (Cu or HT-Cu@PI)) is used to calculate the volumetric energy of the EDLi||NMC622 cells, cells with EDLi-HT-Cu@PI exhibits a higher volumetric energy density (438.1 Wh $L^{-1}$) after cycling compared to EDLi-Bare Cu (282.2 Wh $L^{-1}$, Figure S9b). Figure S9 shows that HT-Cu@PI acts as a host of Li which could maintain the volume of EDLi and maximize the Li utilization to improve the specific volumetric energy density of LMBs.

A porous and dendritic surface and a larger volume change of the LMA reflect the drastic capacity decay of LMB and indicate more side reactions. Hence, the extended cycle life of LMB with EDLi-Cu@PI indicates that a well-developed 3D porous substrate can buffer the volume change of Li during repeated deposition and stripping, largely reduce the effective current density

applied on Li electrode due to the high surface area, improve the uniformity of Li-ion flux, suppress Li dendrite formation, and reduce harmful side reactions between Li metal and the electrolyte. To further verify these benefits of the HT-Cu@PI, X-ray photoelectron spectroscopy (XPS) F1s spectra of the cycled EDLi-Cu are obtained. EDLi-Bare Cu shows a stronger peak intensity at 684.8 eV which corresponds to LiF that is from the decomposition of both LiFSI salt and TTE diluent (Figure 3g). [41] Meanwhile, compared to EDLi-Bare Cu, the cycled EDLi-HT-Cu@PI shows a higher $SO_x$-F peak in the XPS F1s spectra, which is from the LiFSI salt decomposition (Figure 3h) [42]. This result underlines again that EDLi-HT-Cu@PI suppresses side reactions on the surface of the LMA during cycling.

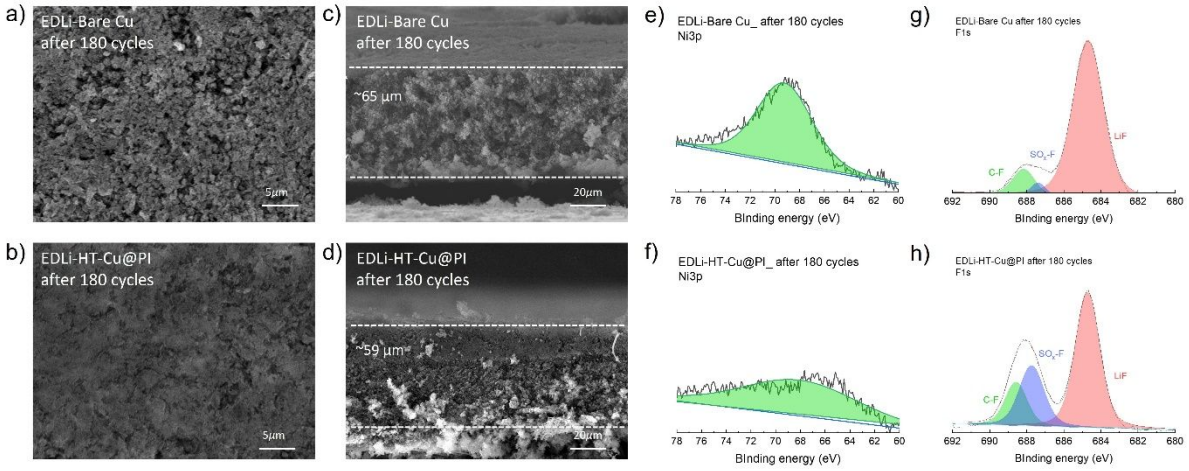


**Figure 3.** Surface view of SEM images of the cycled a) EDLi-Bare Cu and b) EDLi-HT-Cu@PI. Cross-sectional SEM images of the cycled c) EDLi-Bare Cu and d) EDLi-HT-Cu@PI. XPS Ni3p spectra of the cycled e) EDLi-Bare Cu and f) EDLi-HT-Cu@PI. XPS F1s spectra of the cycled g) EDLi-Bare Cu and h) EDLi-HT-Cu@PI.

In recent years, several studies reported the crosstalk from the anode to the cathode in Li-based batteries regarding the anode affects the cathode and this crosstalk could be reduced by a 3D anode substrate. [43, 44] One of the well-known side reactions of Li-based batteries with Ni-rich oxide cathodes is the transition metal ions dissolution (ex. Ni, manganese, and cobalt) resulting in the deposition of the transition metal species on the anode surface by the migration of these metal ions. [45] The deposited species could act as the conduction barrier on the surface of the anode which promotes overpotential and uneven Li flux. The XPS Ni 3p spectra of the cycled EDLi-Bare Cu present a higher intensity of $Ni^{2+}$ which corresponds to the deposited Ni as NiO (Figure 3e) [46] with

higher atomic percent (Table S3) compared to the cycled EDLi-HT-Cu@PI (Figure 3f). Besides, Table S4 summarizes the atomic ratio of NMC622 cathode before and after cycling in EDLi-Cu||NMC622 cells. NMC622 from the cycled cells with EDLi-Bare Cu has less amount of Ni atomic percent because of Ni ion loss while NMC622 cycled with EDLi-HT-Cu@PI maintains most of the Ni concentrations compared to the pristine NMC622. This result shows that HT-Cu@PI contributed to limiting the side reactions on the cathode. Therefore, the alleviated crosstalk influences the structural degradation of the cathode as well.

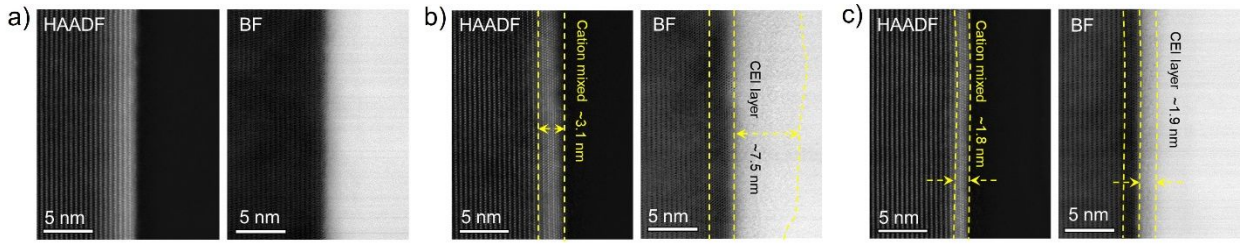


**Figure 4.** STEM images showing structure and CEI characteristics of the NMC622 particles for a) pristine NMC622, b) cycled NMC622 on EDLi-Bare Cu, and c) cycled NMC622 on EDLi-HT-Cu@PI.

Figure 4a shows a fresh NMC622 has no structural degradation. A thicker cation mixing layer (~ 3.1 nm) is observed by using combination of high angle annular dark field (HAADF) and bright field (BF) imaging modes in a scanning transmission electron microscope (STEM) on the NMC622 particles from the cycled EDLi||NMC622 cells with bare Cu compared to the one (~ 1.8 nm) from the cycled cells with HT-Cu@PI (Figure 4b and 4c). In addition, a thinner cathode electrolyte interphase (CEI) layer on the NMC622 particle from cells with HT-Cu@PI (~ 1.9 nm) than that from cells with bare Cu is detected (Figure 4b and 4c). This suggests that the interphase reactions between the cathode and the electrolyte are influenced by variations in the anode. This phenomenon will be subject to in-depth investigation in our future research. These results imply that a 3D HT-Cu@PI strategy for the LMAs could bring higher gravimetric/volumetric energy densities to the LMBs with a stable cycle performance. The structural uniqueness of the 3D HT-Cu@PI current collector that is developed by a facile/versatile method, including enabling both the improved Li-ion transport resulting in better electrochemical performance and the larger mass

loading of electrode active materials leading to increased energy density, as illustrated in Figure 5.

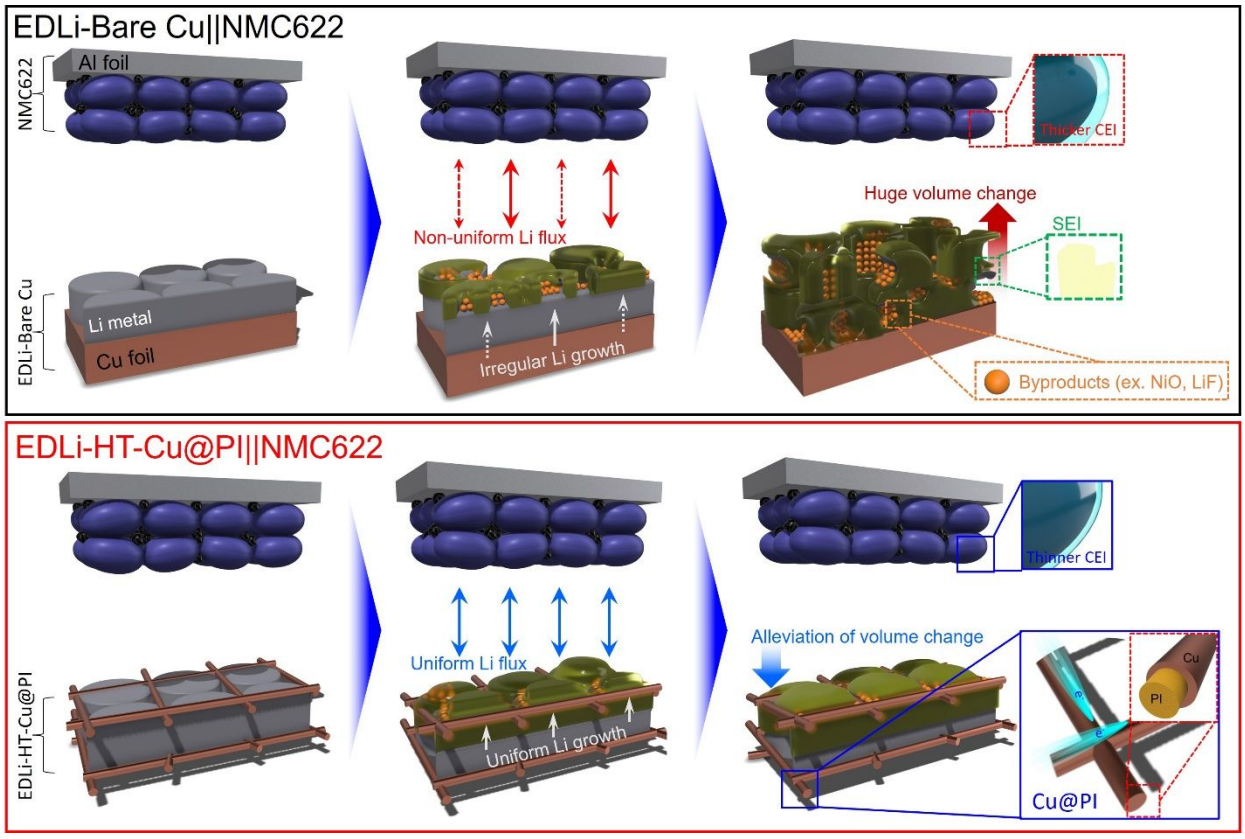


**Figure 5.** Schematic illustration of 3D HT-Cu@PI enhancing Li deposition and battery performance.

In summary, we have developed the 3D-structured HT-Cu@PI current collector as a new platform for the LMAs. The polymeric scaffold was fabricated via electrospinning which is a versatile method to adopt a variety of polymer candidates and PI was selected owing to its high thermal stability. Cu nanoparticles were coated as an electron conduction path provider through the simple electroless plating process. After heat treatment of Cu@PI nanomat at 200 ºC for 10 h to enhance its electronic conductivity, Li was fully deposited inside of the final 3D HT-Cu@PI current collector allowing full utilization of 3D substrate. Driven by boosted Li-ion transport and increased Li nucleation sites, the electrochemically deposited Li on HT-Cu@PI brought increased specific capacity enhanced discharge rate capability and improved cycling stability to the EDLi||NMC622 cells under the closest practical conditions (4.5 mAh $cm^{-2}$ of NMC622, N/P ratio

= 1.11) when compared to the bare Cu. Furthermore, the HT-Cu@PI could alleviate side reactions between LMA and electrolyte that cause Li loss by formation of nonuniform SEI layers, reduce dead Li and volume change of LMA. Benefitting from the lighter weight of HT-Cu@PI and its host role, when the total mass or volume of the cathode, separator, EDLi and anode substrate (Cu or HT-Cu@PI) is considered (the weight of electrolyte, cathode substrate and package materials are not included in this calculation), the EDLi||NMC622 cell with HT-Cu@PI substrate exhibits higher specific energy (382.4 Wh $kg^{-1}$) than that with bare Cu (299.0 Wh $kg^{-1}$). It also exhibits higher specific gravimetric energy density (300.5 Wh $Kg^{-1}$) and a 55% improved volumetric energy density (438.1 Wh $L^{-1}$) than those with bare Cu (152.8 Wh $Kg^{-1}$ and 282.2 Wh $L^{-1}$) even after 180 cycles. We believe that this facile/versatile approach of making 3D-structured metal-thin-film-coated polymeric scaffold as current collector for LMA could enable LMBs toward a higher energy density accompanying a longer stable cycle life.

## ASSOCIATED CONTENT

### Supporting Information

The Supporting Information is available free of charge.

The experimental methods, the electronic conductivity of bare Cu and Cu@PI samples, comparison of electrochemical performance of LMBs, atomic ratio of NMC622 before and after cycling, Cu@PI preparation method, SEM images and EDS mapping of Cu@PI and deposited Li, and specific energy densities of Li||NMC622 cells.

### Note

The authors declare no competing interests.

## ACKNOWLEDGEMENTS

This work is supported by the Assistant Secretary for Energy Efficiency and Renewable Energy, Vehicle Technologies Office of the U.S. Department of Energy (DOE) through the Advanced

Battery Materials Research (BMR) program under the contract no. DE-AC05-76RL01830 for Pacific Northwest National Laboratory (PNNL). The microscopic and spectroscopic characterizations were conducted in the William R. Wiley Environmental Molecular Sciences Laboratory (EMSL), a national scientific user facility sponsored by DOE's Office of Biological and Environmental Research and located at PNNL. Part of the electron microscopy work is carried out by using instruments that are funded in part by a grant from the Washington State Department of Commerce's Clean Energy Fund. PNNL is operated by Battelle for the DOE under Contract DE-AC05-76RL01830. The salt LiFSI was provided by Dr. Kazuhiko Murata of Nippon Shokubai Co., Ltd.

## REFERENCES

(1) Zeng, X.; Li, M.; Abd El-Hady, D.; Alshitari, W.; Al-Bogami, A. S.; Lu, J.; Amine, K. Commercialization of lithium battery technologies for electric vehicles. *Adv. Energy Mater.* **2019**, *9* (27), 1900161.

(2) Sarmah, S.; Lakhanlal; Kakati, B. K.; Deka, D. Recent advancement in rechargeable battery technologies. *Wiley Interdiscipl. Rev.: Energy Environ.* **2023**, *12* (2), e461.

(3) Olabi, A. G.; Abbas, Q.; Shinde, P. A.; Abdelkareem, M. A. Rechargeable batteries: Technological advancement, challenges, current and emerging applications. *Energy* **2022**, 126408.

(4) Zhu, B.; Wang, X.; Yao, P.; Li, J.; Zhu, J. Towards high energy density lithium battery anodes: silicon and lithium. *Chem. Sci.* **2019**, *10* (30), 7132-7148.

(5) Wang, R.; Cui, W.; Chu, F.; Wu, F. Lithium metal anodes: Present and future. *J. Energy Chem.* **2020**, *48*, 145-159.

(6) Ding, J.-F.; Xu, R.; Yan, C.; Li, B.-Q.; Yuan, H.; Huang, J.-Q. A review on the failure and regulation of solid electrolyte interphase in lithium batteries. *J. Energy Chem.* **2021**, *59*, 306-319.

(7) Zhang, Y.; Zuo, T.-T.; Popovic, J.; Lim, K.; Yin, Y.-X.; Maier, J.; Guo, Y.-G. Towards better Li metal anodes: challenges and strategies. *Mater. Today* **2020**, *33*, 56-74.

(8) Luo, Z.; Qiu, X.; Liu, C.; Li, S.; Wang, C.; Zou, G.; Hou, H.; Ji, X. Interfacial challenges towards stable Li metal anode. *Nano Energy* **2021**, *79*, 105507.

(9) Nanda, S.; Gupta, A.; Manthiram, A. Anode-free full cells: a pathway to high-energy density lithium-metal batteries. *Adv. Energy Mater.* **2021**, *11* (2), 2000804.

(10) Guo, Y.; Li, H.; Zhai, T. Reviving lithium-metal anodes for next-generation high-energy batteries. *Adv. Mater.* **2017**, *29* (29), 1700007.

(11) Liu, F.; Xu, R.; Hu, Z.; Ye, S.; Zeng, S.; Yao, Y.; Li, S.; Yu, Y. Regulating lithium nucleation via CNTs modifying carbon cloth film for stable Li metal anode. *Small* **2019**, *15* (5), 1803734.

(12) Zhang, Y.; Liu, B.; Hitz, E.; Luo, W.; Yao, Y.; Li, Y.; Dai, J.; Chen, C.; Wang, Y.; Yang, C. A carbon-based 3D current collector with surface protection for Li metal anode. *Nano Research* **2017**, *10*, 1356-1365.

(13) Cao, J.; Xie, Y.; Li, W.; Wang, X.; Yang, Y.; Zhang, Q.; Guo, J.; Yang, C.; Cheng, S.; Zhang, C. Rationally optimized carbon fiber cloth as lithiophilic host for highly stable Li metal anodes. *Mater. Today Energy* **2021**, *20*, 100663.

(14) Jiang, G.; Jiang, N.; Zheng, N.; Chen, X.; Mao, J.; Ding, G.; Li, Y.; Sun, F.; Li, Y. MOF-derived porous Co3O4-NC nanoflake arrays on carbon fiber cloth as stable hosts for dendrite-free Li metal anodes. *Energy Storage Mater.* **2019**, *23*, 181-189.

(15) Yan, C.; Xu, T.; Ma, C.; Zang, J.; Xu, J.; Shi, Y.; Kong, D.; Ke, C.; Li, X.; Wang, Y. Dendrite-free Li metal plating/stripping onto three-dimensional vertical-graphene@ carbon-cloth host. *Front. Chem.* **2019**, *7*, 714.

(16) Chen, H.; Yang, Y.; Boyle, D. T.; Jeong, Y. K.; Xu, R.; de Vasconcelos, L. S.; Huang, Z.; Wang, H.; Wang, H.; Huang, W. Free-standing ultrathin lithium metal–graphene oxide host foils with controllable thickness for lithium batteries. *Nat. Energy* **2021**, *6* (8), 790-798.

(17) Park, G.-k.; Kang, H.; Lee, J.-W. Fabrication and characterization of Li-coated nickel mesh for anode of lithium-metal batteries. *J. Alloys Compds.* **2019**, *790*, 847-852.

(18) Li, Q.; Zhu, S.; Lu, Y. 3D porous Cu current collector/Li-metal composite anode for stable lithium-metal batteries. *Adv. Funct. Mater.* **2017**, *27* (18), 1606422.

(19) Chi, S. S.; Liu, Y.; Song, W. L.; Fan, L. Z.; Zhang, Q. Prestoring lithium into stable 3D nickel foam host as dendrite-free lithium metal anode. *Adv. Funct. Mater.* **2017**, *27* (24), 1700348.

(20) Lin, K.; Xu, X.; Qin, X.; Zhang, G.; Liu, M.; Lv, F.; Xia, Y.; Kang, F.; Chen, G.; Li, B. Restructured rimous copper foam as robust lithium host. *Energy Storage Mater.* **2020**, *26*, 250-259.

(21) Wu, Q.; Qin, M.; Yan, H.; Zhong, W.; Zhang, W.; Liu, M.; Cheng, S.; Xie, J. Facile Replacement Reaction Enables Nano-Ag-Decorated Three-Dimensional Cu Foam as High-Rate Lithium Metal Anode. *ACS Appl. Mater. Interfaces* **2022**, *14* (37), 42030-42037.

(22) Chen, W.; Li, S.; Wang, C.; Dou, H.; Zhang, X. Targeted Deposition in a Lithiophilic Silver-Modified 3D Cu Host for Lithium-Metal Anodes. *Energy Environ. Mater.* **2023**, *6* (5), e12412.

(23) Hou, Z.; Yu, Y.; Wang, W.; Zhao, X.; Di, Q.; Chen, Q.; Chen, W.; Liu, Y.; Quan, Z. Lithiophilic Ag nanoparticle layer on Cu current collector toward stable Li metal anode. *ACS Appl. Mater. Interfaces* **2019**, *11* (8), 8148-8154.

(24) Liu, T.; Chen, S.; Sun, W.; Lv, L. P.; Du, F. H.; Liu, H.; Wang, Y. Lithiophilic Vertical Cactus-Like Framework Derived from Cu/Zn-Based Coordination Polymer through In Situ Chemical Etching for Stable Lithium Metal Batteries. *Adv. Funct. Mater.* **2021**, *31* (14), 2008514.

(25) Zhang, Z.; Song, Y.; Zhang, B.; Wang, L.; He, X. Metallized Plastic Foils: A Promising Solution for High-Energy Lithium-Ion Battery Current Collectors. *Adv. Energy Mater.* **2023**, *13* (36), 2302134.

(26) Yun, J. H.; Han, G.-B.; Lee, Y. M.; Lee, Y.-G.; Kim, K. M.; Park, J.-K.; Cho, K. Y. Low resistance flexible current collector for lithium secondary battery. *Electrochem. Solid-State Lett.* **2011**, *14* (8), A116.

(27) Ye, Y.; Chou, L.-Y.; Liu, Y.; Wang, H.; Lee, H. K.; Huang, W.; Wan, J.; Liu, K.; Zhou, G.; Yang, Y. Ultralight and fire-extinguishing current collectors for high-energy and high-safety lithium-ion batteries. *Nat. Energy* **2020**, *5* (10), 786-793.

(28) Pan, C.; Chen, S.-J.; Huang, Y.-H.; Wang, L.; Luo, J.-L.; Fu, X.-Z. A facile method to fabricate lightweight copper coated polyimide film current collectors for lithium-ion batteries. *J. Power Sources* **2022**, *528*, 231207.

(29) Wu, X.; Chen, S.; Liu, D.; Ye, C.; Si, F.; Zhang, Y.; Yang, Y.; Luo, J.-L.; Fu, X.-Z. Polymer@ Cu composite foils with through-hole arrays as lightweight and flexible current collectors for lithium-ion batteries. *J. Energy Storage* **2023**, *74*, 109208.

(30) Shacham-Diamand, Y. Y. Electroless copper deposition using glyoxylic acid as reducing agent for ultralarge scale integration metallization. *Electrochem. Solid-State Lett.* **2000**, *3* (6), 279.

(31) Hossain Bhuiyan, M. E.; Moreno, S.; Wang, C.; Minary-Jolandan, M. Interconnect fabrication by electroless plating on 3D-printed electroplated patterns. *ACS Appl. Mater. Interfaces* **2021**, *13* (16), 19271-19281.

(32) Gao, L. T.; Guo, Z.-S. Effects of optimized electrode surface roughness and solid electrolyte interphase on lithium dendrite growth. *Energy Technol.* **2021**, *9* (7), 2000968.

(33) Jiang, Y.; Wang, B.; Liu, P.; Wang, B.; Zhou, Y.; Wang, D.; Liu, H.; Dou, S. Modified solid-electrolyte interphase toward stable Li metal anode. *Nano Energy* **2020**, *77*, 105308.

(34) Zhai, P.; Liu, L.; Gu, X.; Wang, T.; Gong, Y. Interface engineering for lithium metal anodes in liquid electrolyte. *Adv. Energy Mater.* **2020**, *10* (34), 2001257.

(35) Ren, X.; Gao, P.; Zou, L.; Jiao, S.; Cao, X.; Zhang, X.; Jia, H.; Engelhard, M. H.; Matthews, B. E.; Wu, H.; Lee, H.; Niu, C.; Wang, C.; Arey, B. W.; Xiao, J.; Liu, J.; Zhang, J.-G.; Xu, W. Role of inner solvation sheath within salt–solvent complexes in tailoring electrode/electrolyte interphases for lithium metal batteries. *Proc. Natl. Acad. Sci.* **2020**, *117* (46), 28603-28613.

(36) Jiang, M.; Danilov, D. L.; Eichel, R. A.; Notten, P. H. A review of degradation mechanisms and recent achievements for Ni-rich cathode-based Li-ion batteries. *Adv. Energy Mater.* **2021**, *11* (48), 2103005.

(37) Kim, J.-M.; Zhang, X.; Zhang, J.-G.; Manthiram, A.; Meng, Y. S.; Xu, W. A review on the stability and surface modification of layered transition-metal oxide cathodes. *Mater. Today* **2021**, *46*, 155-182.

(38) Elumalai, S.; Joseph, P. L.; Mathiarasu, R. R.; Raman, K.; Subashchandrabose, R. Three-dimensional octahedral nanocrystals of $Cu_2O/CuF_2$ grown on porous Cu foam act as a lithophilic

skeleton for dendrite-free lithium metal anode. *ACS Appl. Mater. Interfaces* **2023**, *15* (36), 42648-42658.

(39) Yuan, H.; Ding, X.; Liu, T.; Nai, J.; Wang, Y.; Liu, Y.; Liu, C.; Tao, X. A review of concepts and contributions in lithium metal anode development. *Mater. Today* **2022**, *53*, 173-196.

(40) Liang, Z.; Lin, D.; Zhao, J.; Lu, Z.; Liu, Y.; Liu, C.; Lu, Y.; Wang, H.; Yan, K.; Tao, X. Composite lithium metal anode by melt infusion of lithium into a 3D conducting scaffold with lithiophilic coating. *Proc. Natl. Acad. Sci.* **2016**, *113* (11), 2862-2867.

(41) Esen, E.; Mohrhardt, M.; Lennartz, P.; de Meatza, I.; Schmuck, M.; Winter, M.; Paillard, E. Effect of prelithiation with passivated lithium metal powder on passivation films on high-energy NMC-811 and $SiC_x$ electrodes. *Mater. Today Chem.* **2023**, *30*, 101587.

(42) Li, Y.; Liu, M.; Wang, K.; Li, C.; Lu, Y.; Choudhary, A.; Ottley, T.; Bedrov, D.; Xing, L.; Li, W. Single-Solvent-Based Electrolyte Enabling a High-Voltage Lithium-Metal Battery with Long Cycle Life. *Adv. Energy Mater.* **2023**, *13* (30), 2300918.

(43) Lee, H.; Lim, H.-S.; Ren, X.; Yu, L.; Engelhard, M. H.; Han, K. S.; Lee, J.; Kim, H.-T.; Xiao, J.; Liu, J.; Xu, W.; Zhang, J.-G. Detrimental effects of chemical crossover from the lithium anode to cathode in rechargeable lithium metal batteries. *ACS Energy Lett.* **2018**, *3* (12), 2921-2930.

(44) Langdon, J.; Manthiram, A. Crossover effects in batteries with high-nickel cathodes and lithium-metal anodes. *Adv. Funct. Mater.* **2021**, *31* (17), 2010267.

(45) Zhan, C.; Wu, T.; Lu, J.; Amine, K. Dissolution, migration, and deposition of transition metal ions in Li-ion batteries exemplified by Mn-based cathodes–a critical review. *Energy Environ. Sci.* **2018**, *11* (2), 243-257.

(46) Tarditi, A. M.; Barroso, N.; Galetti, A. E.; Arrúa, L. A.; Cornaglia, L.; Abello, M. C. XPS study of the surface properties and Ni particle size determination of Ni-supported catalysts. *Surface Interface Anal.* **2014**, *46* (8), 521-529.

(47) Carlberg, B.; Ye, L. L.; Liu, J. Surface-confined synthesis of silver nanoparticle composite coating on electrospun polyimide nanofibers. *Small* **2011**, *7* (21), 3057-3066.